Bull Volcanol (2011) 73:613–630
DOI 10.1007/s00445-010-0428-x

RESEARCH ARTICLE

Tephra stratigraphy and eruptive volume of the May, 2008, Chaitén eruption, Chile

Fabrizio Alfano · Costanza Bonadonna · Alain C. M. Volentik · Charles B. Connor · Sebastian F. L. Watt · David M. Pyle · Laura J. Connor

Received: 11 June 2010 / Accepted: 8 November 2010 / Published online: 7 December 2010

Abstract On May 1st 2008 Mount Chaitén (southern Chile) interrupted a long period of quiescence, generating a sequence of explosive eruptions and causing the evacuation of Chaitén town located a few kilometers south of the volcano. The activity was characterized by several explosive events each associated with plumes which reached up to about 19 km above sea level. The products were dispersed across a wide area, with the finest ash reaching the Atlantic coast of Argentina. Our field observations in the proximal-medial area (3–25 km from the vent) indicate that the May 2008 tephra deposit consists of numerous layers, most of which can be correlated with individual eruptive events. These layers vary from extremely fine-grained ash to layers of lapilli and blocks, composed of both juvenile and lithic material. Here we describe the stratigraphy and physical characteristics of the May 2008 deposits, and propose a reconstruction of the timing of the May 2008 events. The deposits are mainly associated with the three main explosive phases which occurred on 1st–2nd May, 3rd–5th May and 6th May, with an estimated bulk tephra volume of 0.5–1.0 km^3 (integration of both exponential and power-law fitting). For the 6th May event, represented by a layer composed mainly of lithic lapilli and blocks (>2 mm), an isopleth map was compiled from which a 19 km plume height was determined, which is in good agreement with satellite observations.

Keywords Chaitén · Tephra · Stratigraphy · Explosive eruption · Eruptive volume

Editorial responsibility S. Nakada

F. Alfano (✉) · C. Bonadonna
Department of Mineralogy, University of Geneva,
rue des Maraichers 13,
CH-1205, Geneva, Switzerland
e-mail: fabrizio.alfano@unige.ch

A. C. M. Volentik · C. B. Connor · L. J. Connor
Department of Geology - SCA 528, University of South Florida,
4202 E. Fowler Ave.,
Tampa, FL 33620, USA

S. F. L. Watt · D. M. Pyle
Department of Earth Sciences, University of Oxford,
South Parks Road OX1 3AN, UK

Introduction

Before the 2008 eruption Chaitén volcano, located in the northern part of Chilean Patagonia, to the west of the larger Michimahuida volcano, was considered as a long dormant volcanic complex (Naranjo and Stern 2004). It is widely believed that the last known explosive eruption of Chaitén was related to the formation of a 3–4 km diameter caldera at about 9400 ^{14}C years BP (Naranjo and Stern 2004). On the basis of the collapse caldera's volume, this event was estimated to have erupted about 4 km^3 of material. With the rejuvenation of Chaitén in 2008, new work has shown that Chaitén may have been the source of a major Holocene rhyolite pumice unit (Mic2) previously ascribed to Michimahuida, with an age <3,820 yrs BP (Watt et al. 2009). Prior to the 2008 activity, the caldera was partially filled by an obsidian dome, which may have been emplaced >5,600 years ago, on the basis of obsidian of the same composition having been found in nearby archaeological contexts (Stern et al. 2009). In summary, there is growing evidence for previously unknown Holocene eruptions of Chaitén volcano, one of them possibly in the 17th century (Lara, personal commun.).

The first historical eruption of Chaitén volcano began in May 2008 (Lara 2009). Although the volcano was not monitored, the onset of activity appears to have been rapid, within about 36 h of the first felt earthquake (Castro and Dingwell 2009). Deep, but unfelt, seismicity was recorded beneath Chaitén by a temporary network deployed in 2004–2005 (Cembrano and Lara 2009; Lange et al. 2008).

The first major phase of explosive activity took place on May 2nd, but there is evidence that ash emissions began on May 1st, 2008 (Castro and Dingwell 2009). The erupted products are exclusively of a crystal-poor rhyolite, with a glass silica content of 73–76%; a composition which is rare in the Southern Andean volcanic arc (Naranjo and Stern 2004). At the time of writing the eruption continues, having shifted, after the first few days of explosive activity, into an extended dome-forming phase of eruption (Lara, 2009). This is believed to have been the first major explosive eruption of rhyolite since the eruption of Novarupta (Alaska) in 1912 (Houghton et al. 2004; Carn et al. 2009). With so few historical examples of rhyolitic eruptions, it is particularly important to document the onset of Chaitén activity and the associated eruptive dynamics. Other examples of explosive young rhyolite eruptions include Askja 1875 (Sparks et al. 1981) and Taupo 186 AD (Walker 1980).

The dispersal of tephra during the first week of the eruption affected a vast region (with ash deposited over an area>2×10^5 km^2), from Chile to the Atlantic coast of Argentina (Watt et al. 2009). The eruption caused the evacuation of more than five thousand people from a 50 km radius area (Lara 2009), led to the eventual abandonment and relocation of the town of Chaitén, and disrupted agriculture, tourism and aviation (Watt et al. 2009; Martin et al. 2009).

From the distribution of deposits in the distal area of Argentina presented in Watt et al. (2009), the May 2008 eruption of Chaitén is estimated to have generated more than 0.2 km^3 of tephra in the period between May 1st and June 11th 2008. Our goal is to document the proximal–medial stratigraphy (3–25 km from the vent) of the tephra deposit from the early May activity, and relate these layers to the known sequence of explosive events known from direct observations and remotely sensed data. Moreover we want to integrate the data on distal deposits published by Watt et al. (2009) with field observations in the area between Chaitén town (10 km from the vent) and Futaleufù (75 km from the vent), in order to give a more complete description of the deposit produced by the eruption.

The May 2008 tephra deposit consists of numerous layers, most of which can be correlated with specific explosions. The early stages of the eruption produced a complex stratigraphy characterized by at least 14 individual layers. These layers vary from extremely fine-grained ash to layers of lapilli and large blocks of both juvenile and lithic material. No clear deposits of pyroclastic density currents (PDC) were found in the area which was mapped, although patterns of vegetation damage and tree fall on the inaccessible slopes leading up to the dome appear to be consistent with the emplacement of local, damaging PDCs. All of the mapped deposits are interpreted as tephra fall from the main explosive-eruption plumes or from plumes associated with PDCs that flowed through the north-eastern valleys, which were not accessible due to the roughness of the terrain and safety reasons. Seismic data suggest that the extrusion of a new dome, which was first observed on May 21st, started on May 12th (Lara 2009), so it can be inferred that PDCs generated during the onset of the May eruption were associated with column collapse rather than dome collapses.

Although the May eruption was of only moderate volume, tephra fall seriously affected the proximal region by damaging seriously the vegetation of the surrounding forest, depositing very fine grained tephra that was remobilized, and serving as the source of lahars (Lara 2009). Distal areas were affected by fine ash in suspension in the atmosphere, which disrupted air traffic (Martin et al. 2009).

The tephra fall deposit

Our observations of the May tephra fall deposit were made during January 2009, about 8 months after the onset of the eruption, and were made at 69 stratigraphic stations (outcrops and pits) located between 3 and 25 km from the Chaitén dome (Fig. 1). These stations are distributed among four traverses, two located SE of the vent and two located N of the vent, and accessed by vehicle or on foot. Sample locations were limited by the rugged terrain and a dense temperate rainforest that surrounds Chaitén volcano. No sites within ~3 km of the vent were visited for safety reasons. Evidence of reworking was observed only for the top layers (N-O in the southeast sector, $o-\pi$ in the north sector), while the bottom and middle layers showed consistent values of thickness throughout the exposed deposit.

Traverses of the southeast side of the volcano are located along the ~N-trending valleys of Rio Amarillo and Rio Michimahuida, about 15 km and 20 km from the volcano, respectively (Fig. 1). The station points along the Rio Amarillo traverse follow the “Ventisquero el Amarillo” trail. At the time of the fieldwork, access to this area was seriously compromised due to a flood that covered the lowest part of the valley (area between RA01 and RA11) and from trees fallen across the trail, which had been topped by the weight of accumulated tephra accumulation (area between RA11 and RA02). Starting from the base camp located in RA08, where the “Sendero el Crater” trail begins, the trail was very easy to walk. The traverse stops at

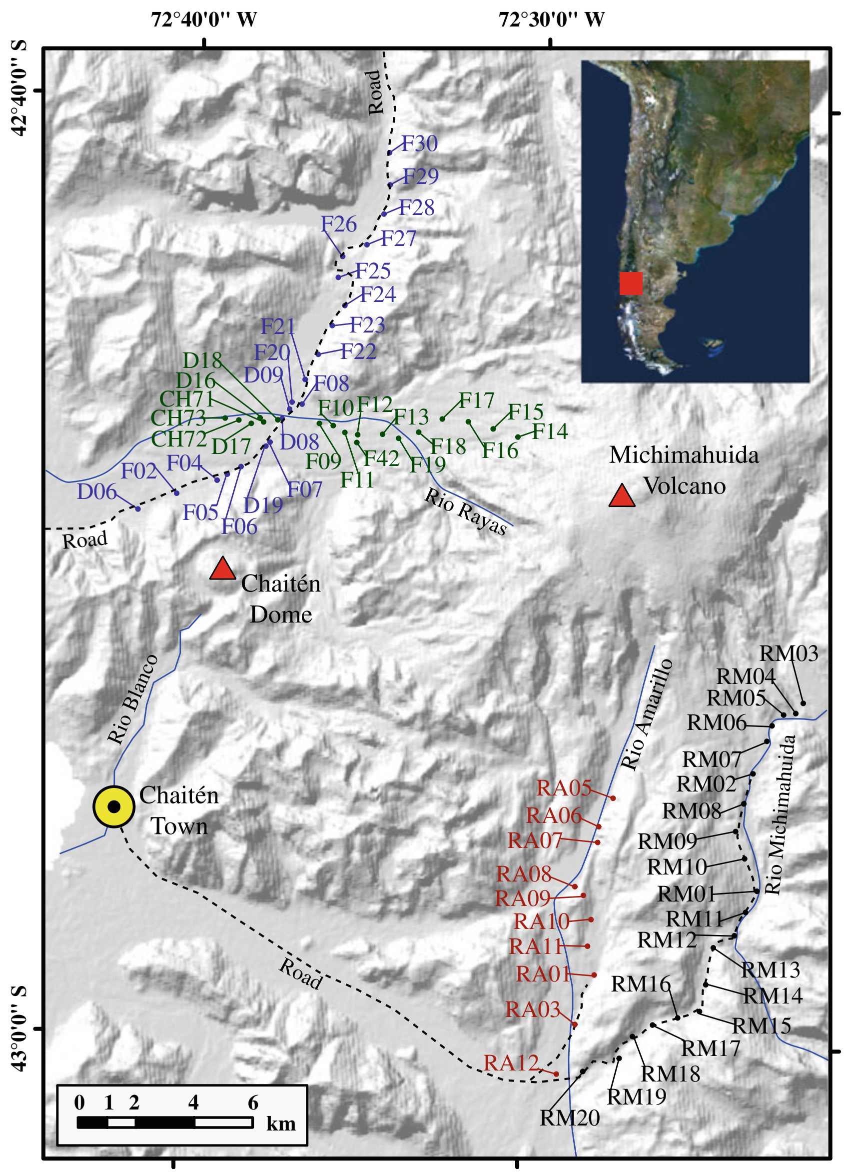

Fig. 1 Map of the area around Chaitén volcano showing the four traverses in the southeastern sector (*black* and *orange* points) and on the northern sector (*green* and *blue* points). Dashed lines indicate the main roads and paths that provide access to the proximal and medial deposit

the station RA05 where it was not possible to go further due to the impassable Rio Amarillo. The station points along the Rio Michimahuida traverse follow a N-S dirt road which crosses N-S the valley and stops at the station point RM02. To reach the station points RM07 to RM03 it was necessary to cross the Rio Michimahuida. Tephra deposits in the SE sector are thickest along the Rio Amarillo, where they reach thicknesses of about 23 cm at stratigraphic station RA07 (16 km from the vent). The maximum thickness reached along the Rio Michimahuida is about 16 cm at stratigraphic station RM13 (21 km from the vent; Fig. 1).

Stratigraphic stations located on the north side of the volcano are 3–15 km from the vent along a N-S trending road and along the “Sendero Michimahuida” trail, located south of the Rio Rayas (Fig. 1). The station points along the N-S trending traverse are mainly located next to the road, and are easily accessible by car. The points between CH73 and CH71 are located inside the area of the camp ground “El Volcan”. The points between F09 and F14 are located along the Sendero Michimahuida, which leads up to the northwest side of the Michimahuida glacier, in a forest area located south to the Rio Rayas. This forest, in the period of the fieldwork, was heavily covered by volcanic ash, which made it difficult to follow the trail.

Total tephra deposits in this area reach a maximum thickness of 23 cm at location D19 along the N-S traverse, and 26 cm at location F12 on the E-W traverse (Fig. 1).

Stratigraphy of the southeast sector

A total of 16 layers, named from A to P are identified in the SE sector (RM08; Fig. 2a). The most complete sequence of

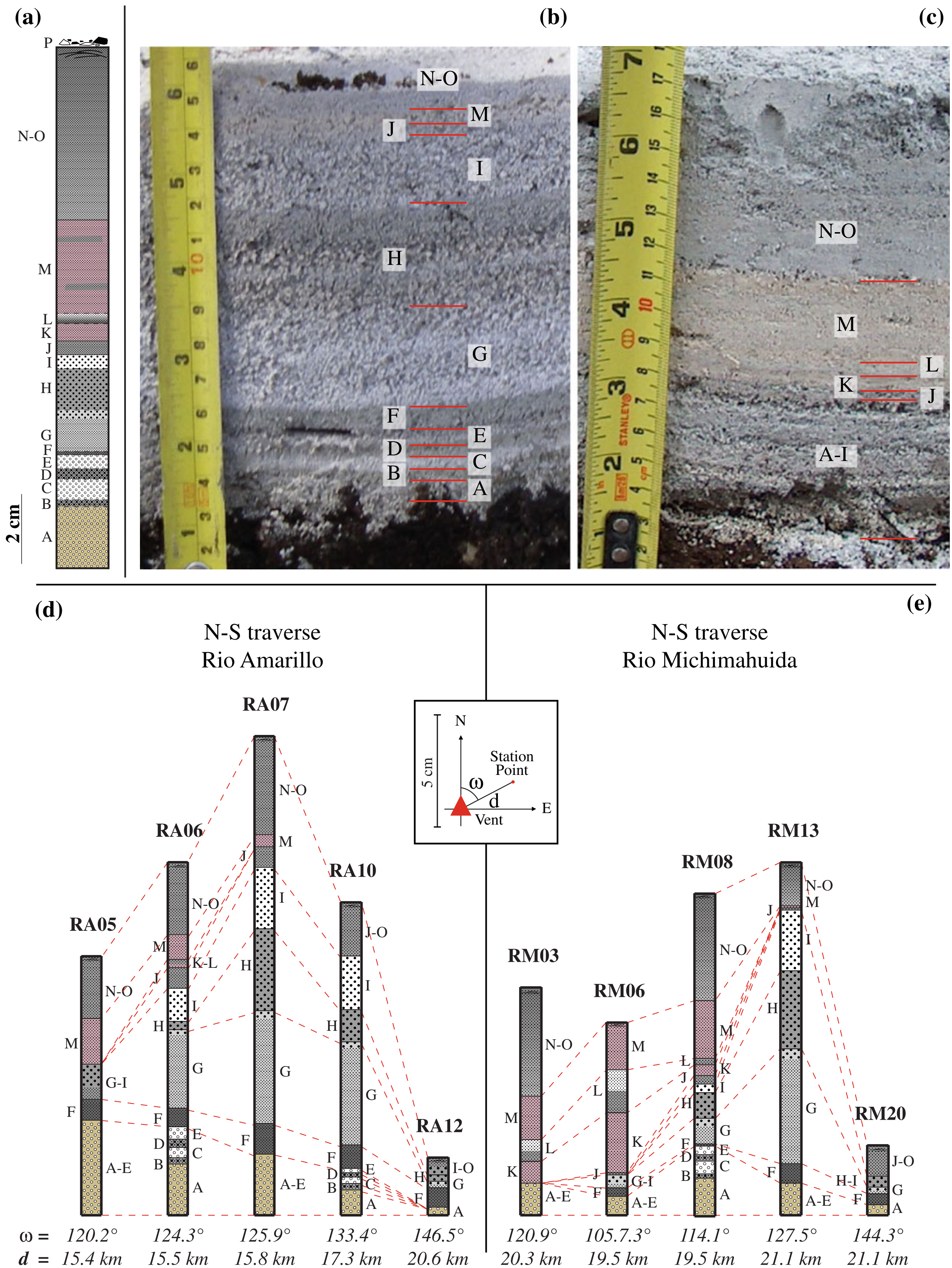

(a)
(b)
(c)
2 cm
N-O
M
L
K
J
I
H
G
F
E
D
C
B
A
A-I
(d)
N-S traverse
Rio Amarillo
RA05
RA06
RA07
RA10
RA12
(e)
N-S traverse
Rio Michimahuida
RM03
RM06
RM08
RM13
RM20
N
E
Station Point
ω
d
Vent
5 cm
ω = 120.2° 124.3° 125.9° 133.4° 146.5° 120.9° 105.7.3° 114.1° 127.5° 144.3°
d = 15.4 km 15.5 km 15.8 km 17.3 km 20.6 km 20.3 km 19.5 km 19.5 km 21.1 km 21.1 km

◀ **Fig. 2** Stratigraphy of the southeast sector. **a** Reference section for the southeastern sector (stratigraphic station RM08). The section is composed, from bottom to top, of the following layers: *A*, coarse ash layer, 60% pumices with average grain size of 1 mm, well sorted and without matrix; *B*, fine to coarse gray ash, lithic rich; *C*, coarse ash, well sorted, white pumice-rich (90%); *D*, fine to coarse gray ash, lithic rich; *E*, coarse ash, well sorted, white-pumice rich (90%); *F*, fine gray ash; *G*, light fine gray ash grading up to coarse white ash; *H*, gray coarse ash; *I*, white coarse ash; *J*, fine gray ash; *K*, fine pink ash; *L*, fine banded ash, gray on bottom and white on top; *M*, fine pink massive ash with some discontinuous gray layers; *N*, fine light-gray ash; *O*, dark gray ash, often reworked; *P*, scattered pumices lapilli on surface. **b** stratigraphic station RM12 showing a very good exposure of the layers A-I; **c** stratigraphic station RM08 showing all the layers present in the southeastern sector. **d** Stratigraphic sections along the Rio Amarillo traverse. **e** Stratigraphic sections along the Rio Michimahuida traverse

layers in the southeastern sector is visible at locations RM08 and RM12 (Fig. 2b and c). The sequence lies conformably on soil and shows no evidence of reworking and contains no accretionary lapilli. The layers were distinguished from one another in the field by changes in color and grainsize. Occasionally these changes are abrupt, but other transitions are gradational. Layers J-O are missing in some sections, presumably due to erosion prior to deposition of P.

A summary of the variation in thickness of the layers of the southeastern sector as measured in the most relevant stratigraphic stations, with polar coordinates, to the vent, is shown in Fig. 2d and e. The sections reported show the end points of the two traverses (RA05-RA12 and RM03-RM20; Fig. 1), the stations with maximum cumulative deposit thicknesses (RA07 and RM13; Fig. 1), the stations with the maximum cumulative thicknesses of the A-I layers (RA07 and RM13; Fig. 1) and the station with the maximum cumulative thicknesses of the layers K-M (RA05 and RM06; Fig. 1).

The succession starts with Layer A, which rests directly on the pre-eruption soil (or the pre-eruption leaf litter) and consists of very well sorted coarse ash with ~60% pumice and ~40% lithic fragments and no matrix (all componentry information given in this paper is based on macroscopic field observations). Above this layer there is a sequence of alternating fine- and coarse-ash layers (B to O). These layers show in general gradational contacts, with the exception of layers E-F which have sharp contact. Thickness maxima could be identified for the layer-sequence A-J along both traverses: 17 cm along Rio Amarillo (RA06; Fig. 1) and 14 cm along Rio Michimahuida (RM13; Fig. 1). The variation in thickness, as clearly shown in Fig. 2b and c, seems to indicate that the sequence A-J was deposited under similar meteorological conditions. The stratigraphic stations where the maximum thickness is reached (RA06 and RM13; Fig. 1) are both located SE of the crater.

A package of three massive ash layers lies above the A-J layers: a pink fine ash layer at the bottom, K; a layer of fine ash in the middle which varies from white to gray, L; a pink fine ash layer at the top, M. The sequence K-M has a clear maximum thickness of 7 cm along the Rio Michimahuida (RM06; Fig. 1). It was not possible to determine the thicknesses of K-M along the Rio Amarillo traverse as we could not sample further north due to the rough terrain in this area. The maximum thickness observed along the Rio Amarillo traverse is <2.2 cm (RA05; Fig. 1), but from the trend toward increasing along this traverse, and the distribution of the products along the Rio Michimahuida traverse, it is reasonable to infer a maximum thickness of this sequence somewhere north of the stratigraphic station RA05, along the W-E line between the crater and stratigraphic station RM06. The consistency in thickness variation for the layers K-M indicates that the layers were deposited under similar wind conditions, producing a narrow deposit oriented towards E.

Layers N-O do not have clear maxima and consist of many laminations reflecting variable wind conditions during deposition, with possible reworking during prolonged exposure. Each lamina is interpreted to represent a single explosive event of very low volume, accumulated in the months prior to January 2009 (when we made our field observations).

Stratigraphy of the north sector

The section for the deposit in the N sector consists of 18 layers. The sequence lies conformably on soil, no evidence of reworking, and contains no accretionary lapilli. The most complete succession of the layers characteristic of the northern sector is preserved at locations F14 and F13 (Fig. 3a, b and c). Location F14 (Fig. 1), located 1 km west of the Michimahuida volcano contains 15 of these layers, but lacks layers ο, ν^* and θ. A summary of the variation in thickness of the layers of the north sector as measured in the most relevant stratigraphic stations with polar coordinates (referred to the vent) of their location is shown in Fig. 3d and e. The sections reported show the extreme points of the two traverses (CH73-F14 and F24-D06; Fig. 1), the stations with maximum cumulative thickness of the deposit (F09 and D19; Fig. 1), the stations with the maximum thickness of Layer α (F42), and the station with the maximum thickness of Layer β (F9 and D19; Fig. 1).

The earliest tephra fall deposit on the northern sector of the volcano, Layer α, consists of buff-colored fine ash with lithic clasts of lapilli size at the very base in the most proximal sections. Layer α, which can be observed only along the W-E traverse, reaches a maximum thickness of 5 cm oriented ENE of the crater (F42; Fig. 1).

Layer β is stratigraphically above α and represents the thickest layer of the whole sequence. The unit comprises

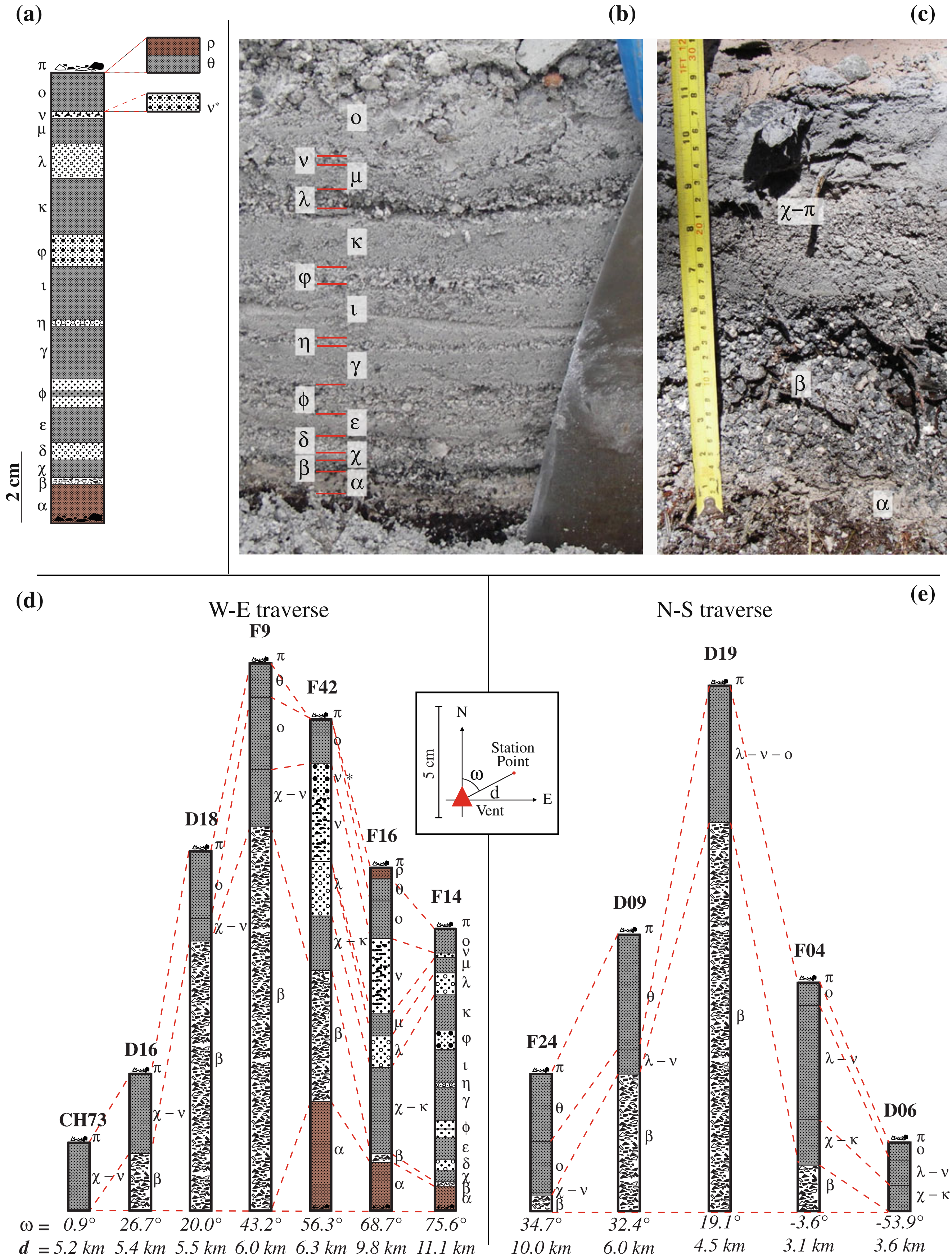
(a)
(b)
(c)
(d)
(e)
2 cm
W-E traverse
N-S traverse
CH73
D16
D18
F9
F42
F16
F14
F24
D09
D19
F04
D06
N
E
5 cm
Station Point
ω
d
Vent
ω = 0.9° 26.7° 20.0° 43.2° 56.3° 68.7° 75.6°
d = 5.2 km 5.4 km 5.5 km 6.0 km 6.3 km 9.8 km 11.1 km
34.7° 32.4° 19.1° -3.6° -53.9°
10.0 km 6.0 km 4.5 km 3.1 km 3.6 km
χ−π
λ − ν − o
χ − ν
χ − κ
λ − ν

Fig. 3 Stratigraphy of the north sector. **a** Reference section for the northern sector (stratigraphic station F14) showing all the layers present in this sector, excepting only the layers ν^*, θ and ρ; the section is composed, from bottom to top, of the following layers: α, basal buff, brownish ash with lithic fragments at the base; β, lapilli layer, 80% lithic; χ, fine gray ash; δ, coarse white ash, pumice rich; ε, fine gray ash; φ, coarse white ash with gray bands; γ, fine gray ash; η, coarse ash and lapilli, 60–70% pumices; ι, fine gray ash; ϕ, white coarse ash and lapilli; κ, fine gray ash; λ, coarse ash and lapilli, 50% pumices, 50% lithics; μ, fine gray ash; ν, coarse white ash with obsidian lithics; ν^*, white coarse ash and lapilli, o, fine gray ash; ρ, brown fine ash; θ, fine gray ash; π, scattered pumice lapilli on surface. **b** stratigraphic station F14. **c** stratigraphic station F13 showing a very good exposure of Layer β on top of Layer α. **d** Stratigraphic sections of the W-E traverse. (e) Stratigraphic sections of the N-S traverse

approximately 80% lithics, 10% obsidian and 10% pumice. Lithics are rhyolitic, with a range of textures, most commonly foliated. A minor proportion of oxidised (red) lithics are also present. The basal half of this unit contains extremely coarse and often flattened lithics, which are absent in the upper half. The upper half of the unit is also slightly richer in pumices. Pumice content increases very slightly in the downwind direction. This layer is massive, and up to 17 cm thick along the W-E and the N-S traverses (respectively in F09 and D19; Fig. 1). As shown in Fig. 1d and e, the variation in thickness of this layer indicates a dispersal axis northeastward from the crater.

Layers χ−ρ are distinguished from one another by changes in color and grainsize. These changes are abrupt in some cases, but other transitions are gradational. The section is mainly characterized by alternation of fine ash and lapilli with a predominance of the juvenile component. Layers from ο to ρ often show reworking, inferred to result from prolonged exposure. Scattered lapilli on the surface are found at the top of this section at many stratigraphic stations (Layer π). No clear thickness maxima have been found for these layers, indicating that they were deposited during different eruptive stages and in different wind conditions. Each layer is interpreted to represent a single explosive event of very low volume.

Overall, the stratigraphic stations on this side of the volcano are characterized by coarser deposits than found in the traverses on the SE of the Chaitén dome.

Chronology of the eruption and correlation with tephra dispersal

Chronology of May 2008 events

Before the eruption of May 2008, Chaitén volcano was unmonitored, due to its long quiescence and lack of historical unrest. The chronology of the May 2008 main events is as follows (reported by Smithsonian weekly report and the SERNAGEOMIN reports):

April 30th–May 1st	A volcano tectonic (VT) seismic event up to a maximum of magnitude 5 is registered by six seismic monitoring stations, located up to 300 km from Chaitén volcano.
May 1st–2nd	The VT activity increases to 20 events per hour in coincidence with the beginning of the eruption, which occurred at 23:38 local time on May 1st, producing a 13–16 km eruptive column sustained for 6 h (Folch et al. 2008; Lara 2009). The ash is dispersed towards the N and SE. The first observers of the erupting volcano reported the presence of an active crater of ~200 m radius located on the N side of the dome, and of an inactive crater of ~400 m radius, located on the NE side of the dome.
May 3rd–May 5th	A 10 km high sustained plume drifted from SE to E reaching the Atlantic coast of Argentina (Watt et al. 2009; Folch et al. 2008; Lara 2009; Carn et al. 2009).
May 6th	Between 8:20 and 9:15 local time, the eruption became more forceful, producing a wide and dark gray ash plume about 20 km high (Watt et al. 2009; Carn et al. 2009; Lara 2009; Folch et al. 2008). The explosion generated a single crater with a radius of ~800 m and was followed by a sequence of explosive events of decreasing intensity.
May 7th–8th	Seismicity at Chaitén increased and a new explosive event was reported but cloudy weather prevented visual observations of the characteristics of the explosion (Watt et al. 2009; Folch et al. 2008).
After May 8th	The intensity of the explosive activity decreased and only ash and steam plumes <10 km high were produced, associated with small dome collapses and/or lateral blasts with associated PDCs that burned

	the forest on the north-eastern side of the volcano.
May 12th	Seismic data suggest initial extrusion of a lava dome, although it was first observed on May 21st (Lara 2009).
May 13th	Production of a lahar which travelled along Rio Blanco reaching the sea damaging about 40 houses in Chaitén town.

At the time of writing (October 2010), Chaitén remains active and the associated eruption is characterized by the growth and collapse of the new dome with production of small plumes and related tephra-fall and block-and-ash flows.

Correlation of tephra layers with the chronology of the eruption

Isopach maps have been compiled for layers A-M (SE sector), α and β (N sector) (Fig. 4).

The sector southeast of the volcano (Fig. 4a) is characterized by a complex succession of relatively thin layers, ranging from a few mm to several centimeters of thickness, that were deposited under similar conditions of wind direction and intensity. The transition between layers is generally gradational, suggesting a prolonged and continuous ash emission, but it is not clear if the activity is best interpreted as a sustained pulsating phase or a sequence of single small explosions. The sequential deposition of A-J (drifted to SE) and K-M (drifted to E) suggests a shift in the wind direction as described for the activity between the 3rd and 5th May by the Smithsonian Institute reports and indicated by the satellite images published by the NASA Earth Observatory (http://earthobservatory.nasa.gov/).

The sector north of the volcano is characterized by a succession of layers even more complex than the SE sector. An isopach map for the whole N sector deposits cannot be drawn because of the inconsistent thicknesses distribution of the cumulative deposits. This can be related to tephra sedimentation under variable wind conditions. It was possible, however to compile isopach maps for the individual layers α and β (Fig. 4b and c), that show a distribution oriented respectively towards ENE and NE. The characteristics of these two deposits, which show an abrupt change in grain size distribution, suggest that they may be related to two different explosive events. The stratigraphic position and the grain size features of Layer α suggest a relation of this layer to the beginning of the eruption on May 1st–2nd, as its dispersion is consistent with what is reported for the initial plume by the Smithsonian Institute and the SERNAGEOMIN. On the other hand, Layer β, which forms the thickest layer and has the coarsest grainsize, can be related to the most powerful phase of the eruption. Moreover, Layer β shows a distribution of products compatible with the characteristics of the climactic event of May 6th described by the Smithsonian Institute and by the satellite images published by the NASA Earth Observatory. The upper layers of the northern sector (χ−π) represent the moderate activity between May 7th 2008 and January 2009 (fallout generated by both explosions and dome collapses).

Fig. 4 Isopach maps (cm) for **a** the layers A-M, showing also the variation in the rotation of the wind direction during the deposition of the layers A-J and K-M; **b** Layer α; **c** Layer β

The total deposit

Integrating the distal thickness measurements presented by Watt et al. (2009) with our new thickness data, a new isopach map of the total deposit was compiled, covering the proximal region and redrawn over distal areas to define a smooth deposit shape comprising two main lobes (Fig. 5). All of the tephra (Fig. 5a) was dispersed eastward from the volcano, covering a wide area and affecting a large part of Argentina: one lobe is oriented ESE and the second ENE. The SE lobe is related to the activity of May 3rd-5th and the ENE lobe to that of May 6th respectively (cf. Watt et al., 2009). On the basis of the correlations described in the previous paragraph, the May 3rd–5th lobe has been associated with the A-M layers deposit and the May 6th lobe with Layer β. Tephra accumulated in Futaleufù to a few centimeters (between 2.5 and 5 cm; Fig. 5b), and based on some revisited locations in Argentina, there was not a significant reduction in thickness compared to the values reported by Watt et al. (2009). This amount of tephra was enough to cause problems for cattle in this area as reported by the local population. Chaitén town has been affected by sedimentation of a few centimeters of tephra, which did not cause significant damage to roof structures (Fig. 5c).

Results

Tephra chemistry

Proximal tephra samples, from the units β, A, G, I, J, M, N and P were analysed and found to be identical in their glass major element chemistry (summarised in Table 1). As well as pumice and obsidian grains, deposits contained finely crystalline lithics that have rhyolitic composition similar to the juvenile glasses. Compositions of both pumice and obsidian glasses form an extremely tight cluster, and are chemically indistinguishable; both are considered to be

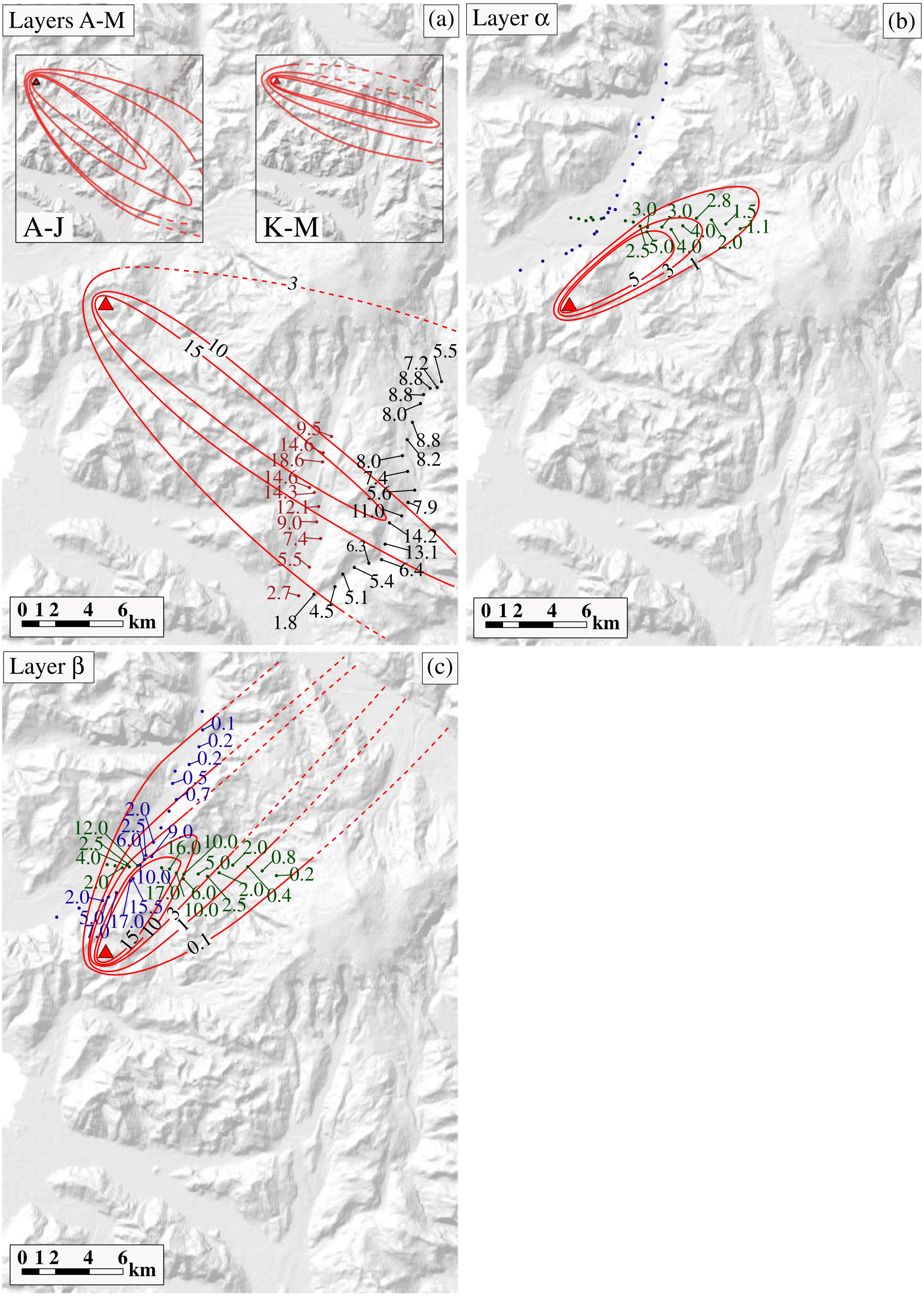

Layers A-M
(a)
A-J
K-M
3
15
10
9.5
14.6
18.6
14.6
14.3
12.1
9.0
7.4
5.5
2.7
1.8
4.5
5.1
5.4
6.3
6.4
13.1
14.2
11.0
7.9
5.6
7.4
8.0
8.2
8.8
8.0
8.8
8.8
7.2
5.5
0 1 2 4 6 km
Layer α
(b)
3.0
3.0
2.8
1.5
1.1
2.0
4.0
4.0
5.0
2.5
5
3
1
0 1 2 4 6 km
Layer β
(c)
0.1
0.2
0.2
0.5
0.7
2.0
2.5
6.0
9.0
12.0
2.5
4.0
2.0
16.0
10.0
2.0
0.8
0.2
5.0
10.0
17.0
6.0
2.0
0.4
10.0
2.5
2.0
5.0
7.0
17.0
15.5
15
10
3
1
0.1
0 1 2 4 6 km

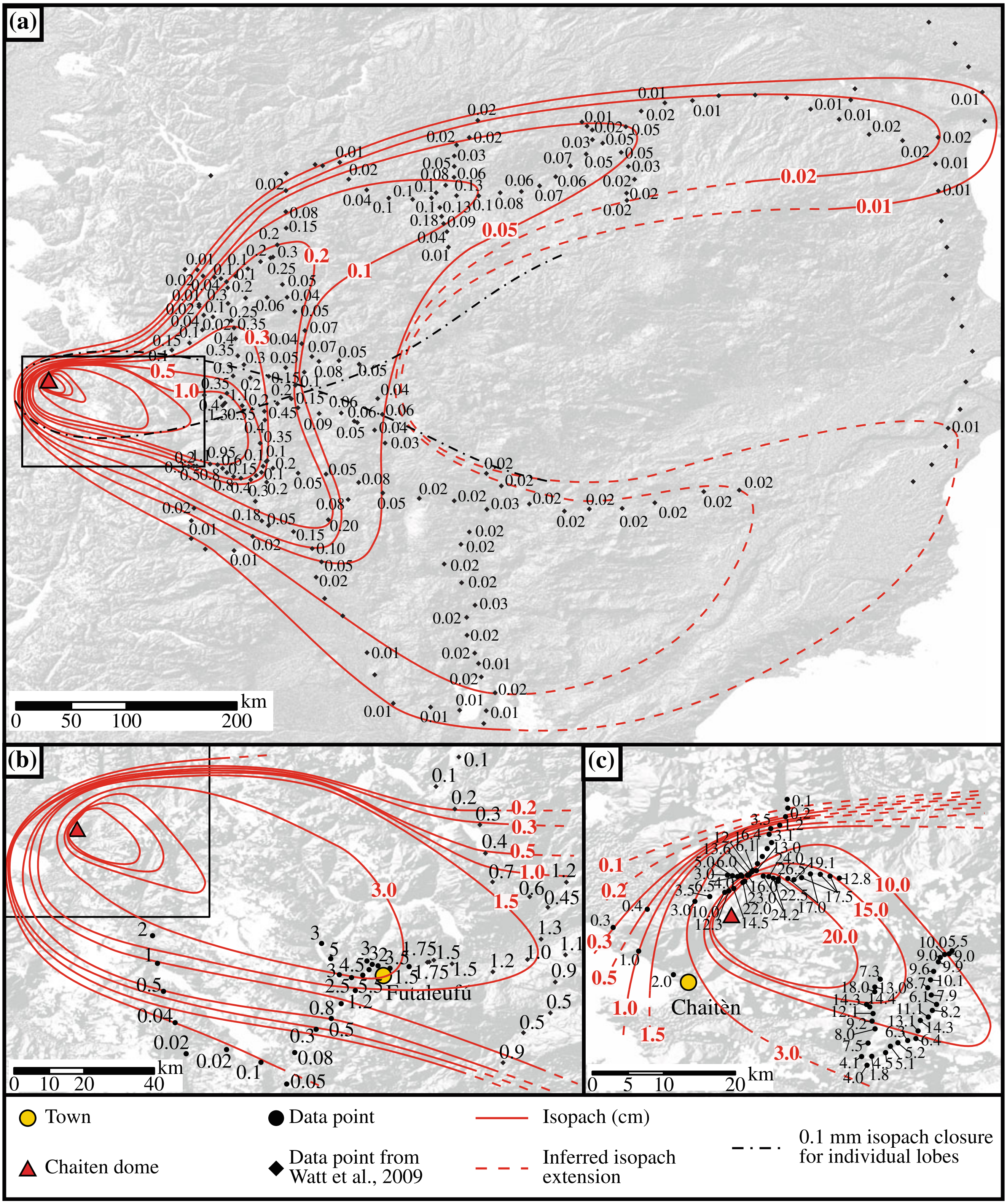

Fig. 5 Isopach maps of the total deposit obtained integrating the new proximal/medial data points and the distal data in the area of Futaleufù (*black circles*) with the data points from Watt et al. (2009) (*green diamonds*), at different scales of observation: **a** total deposit; **b** medial/distal area; **c** proximal/medial area

Table 1 Glass compositions of Chaitén tephra

Unit[a] Location	β (pum.)[b] F09	β (obs.) F09	A RA08	G RA08	I RA08	J RA08	M RA08	N RA08	P RA06	Old Cha. (obs.) F02
N	11	6	5	7	6	9	8	8	10	10
SiO2	74.18	74.11	73.79	74.60	74.57	74.33	74.26	74.77	74.78	76.13
TiO2	0.15	0.16	0.14	0.12	0.15	0.14	0.14	0.15	0.14	0.09
Al2O3	13.66	13.60	13.81	13.79	13.80	13.98	13.68	13.98	13.73	13.24
FeO	1.26	1.21	1.29	1.27	1.25	1.30	1.29	1.32	1.27	1.15
MnO	0.08	0.08	0.07	0.04	0.07	0.07	0.04	0.05	0.06	0.06
MgO	0.28	0.23	0.25	0.27	0.23	0.24	0.26	0.26	0.23	0.18
CaO	1.33	1.33	1.29	1.32	1.38	1.35	1.34	1.36	1.33	0.93
Na2O	3.99	3.84	3.84	3.82	3.92	3.88	3.93	3.84	3.86	3.60
K2O	3.10	3.10	3.08	3.20	3.14	3.17	3.25	3.15	3.16	3.44
Total	98.03	97.65	97.56	98.43	98.52	98.47	98.19	98.88	98.56	98.83

[a]Analyses by electron microprobe, with a 5 µm spot size, at 15 kV and a 4 nA beam current. Only analyses with totals 97–100% included.

[b]All analyses for glass fragments in 2008 ash deposit, unless noted as pumice (pum.) or obsidian (obs.) lapilli, or older Chaitén pyroclastic fall deposit (Old Cha.).

juvenile. Samples of obsidian fragments from older Chaitén pyroclastic fall deposits (collected in location F02; cf. Fig.1) are marginally more silica-rich, and subtly distinct in major element chemistry, differentiating them from juvenile samples. The overall magma composition of the main phase of the 2008 eruption is extremely homogeneous. Of the 70 analyses, all data fall between 73.0 and 75.5 wt% SiO2.

Volume of the deposits

The volumes of Layer α, layers A-M, Layer β and the total deposit have been calculated by exponential fitting and power-law fitting (Pyle 1995; Bonadonna and Houghton 2005; Fig. 6) derived from semi-log plots of thickness vs. square root of the area of the isopach contours of Figs. 4 and 5.

Three exponential segments have been identified for all the deposits studied, except Layer α. For the power-law method the proximal integration limit $\sqrt{A_0}$ has been set equal to 1 km. The distal limit $\sqrt{A_{dist}}$ has been set equal to the square root of the area of the minimum thickness isopach (i.e. minimum thickness of 0.1 mm). For Layer α, the distal limit has been considered variable between 100 and 500 km because no distal data are available (minimum thickness: 1 cm).

Volumes resulting from the integration of the exponential and power-law fitting are respectively 26.8×10^{-4} km^3 and $55.1\pm0.2\times10^{-4}$ km^3 for Layer α considering only proximal data, 2.8×10^{-1} km^3 and 2.4×10^{-1} km^3 for layers A-M integrated with the May 3rd–5th lobe, 2.1×10^{-1} km^3 and 1.4×10^{-1} km^3 for Layer β integrated with the May 6th lobe, and 4.9×10^{-1} km^3 and 9.6×10^{-1} km^3 for the total deposit. The results are summarized in Table 2.

We could not characterize the volume associated with the post-May 6th activity as this is not well described by our stratigraphy due to the fact that these layers were difficult to correlate. The general thicknesses of layers K-M and χ−π suggest that their volumes are probably lower than expected from the May 1st–May 6th activity. As a result, we conclude that the 6th May 2008–January 2009 activity is associated with a volume <0.5 km^3.

Eruptive parameters and classification

The column height for Layer β was determined following compilation of two isopleth maps (Fig. 7): one map based on the geometric mean of the three orthogonal axes of the 5 largest lithics (i.e. 3/5 average technique; Fig. 7a), and one based on the 50th percentile of the average of the three axes of the 20 largest lithics (Fig. 7b). The 50th percentile method was suggested as an alternative to the measurement of the maximum clast by the IAVCEI Commission on Tephra Hazard Modelling because it provides more stable results and it better deals with outliers (http://www.ct.ingv.it/Progetti/Iavcei/index.htm). However, the 50th percentile technique needs an accurate calibration because it inevitably underestimates the plume height if the method of Carey and Sparks (1986) is applied. Here we present an application of this technique to compare it with the more commonly used 3/5 averaging technique. The plume heights determined from measurement of the downwind and crosswind range from the 3.2 cm isopleth line of the two maps are 19 and 17 km respectively (Carey and Sparks 1986). For layers α and A-M, the column height was assumed to be equal to 13 and 10 km, as determined by remote sensing analyses and reported by the Smithsonian Institute (Lara 2009; Folch et al. 2008) (Table 2).

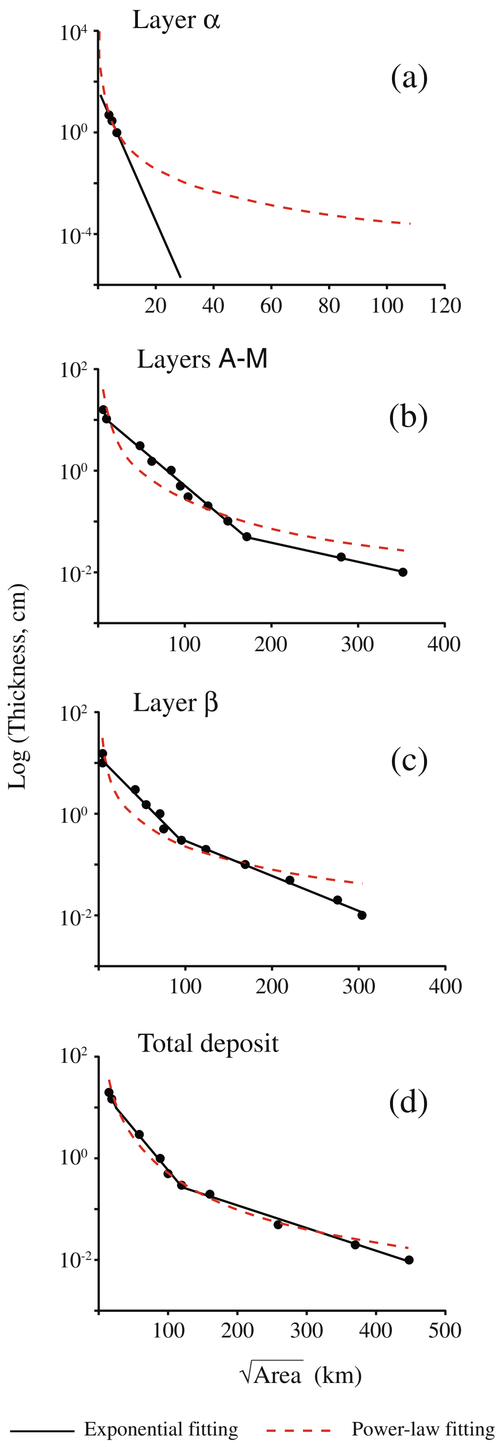

Fig. 6 Semi-log plots of the thinning trends showing the exponential and power-law fits for Layer α (**a**), layers A-M integrated with the 3rd May lobe (**b**), Layer β integrated with the 6th May lobe (**c**) and the total deposit (**d**)

The peak mass eruption rate (MER) for each phase was calculated from the column height values (Wilson and Walker 1987). The resulting MER is 9.2×10^6 kg/s for Layer α, 3.2×10^6 kg/s for layers A-M, 4.2×10^7 kg/s for Layer β. For layer α, the average MER is calculated from the observed eruption duration of the eruptive phase described by the SERNAGEOMIN report (i.e., 6 h), resulting in 1.2×10^5 kg/s. All values are summarized in Table 2.

The durations of different eruption phases (calculated dividing the erupted mass, derived though exponential and power-law volumes respectively, by the mass eruption rate) are about 5 and 10 minutes for Layer α, 25 and 22 h for layers A-M, and 2 and 1 h for Layer β (Table 2).

Layer α (May 1st–2nd), layers A-M (May 3rd–5th) and Layer β can be classified as subplinian, based on the thickness and maximum size half distances (Pyle 1989; Fig. 8a). Moreover, the thinning trends fall in a field of values delimited by the trends of other subplinian eruptions (e.g. Fuego 1974, Mount St. Helens 22 July 1980, Etna 1998 and Ruapehu 1996; Fig. 8b).

Discussion

Eruptive parameters

The explosive phase of the May 2008 Chaitén eruption deposited several tephra layers of variable thickness that in some cases could not be isolated and correlated with sufficient confidence to produce individual isopach maps. Where thin layers had a similar dispersal, however, a cumulative volume could be determined despite their small individual thicknesses (e.g., layers A-M). Layers A-M can be related to a continuous emission of ash associated to a single sustained plume with a variable MER, or to several small plumes related to different fall events. As a result, the dispersal pattern is better described as a combination of layers. In contrast, individual isopach maps could be compiled for layers α and β because they were associated with larger eruptive events.

Combining our proximal-deposit data with the distal-deposit data of Watt et al. (2009), layers A-M and Layer β could be fit both by three exponential segments and by a power-law curve (Fig. 6b and c), resulting in larger volumes. In contrast, Layer α, could only be fit by one exponential segment because distal data are missing. The resulting volume is 20% lower than the value obtained through the power-law fitting. Thus this value can be considered only as a minimum estimate of erupted volume. Layer α is characterized by a power-law exponent >2, typical of small deposits, so the uncertainty regarding the distal integration limit does not affect significantly the volume estimate. In contrast, the integration of the power-law fit associated with the Layer β and layers A-M are more sensitive to the distal integration limit (i.e., power-law exponent <2, typical of wide-spread deposits), making the

Table 2 Summary of the eruptive parameters of the May 2008 activity

Unit	α (May 1st–2nd)	A-M (May 3rd–5th)	β (May 6th)	Total deposit
Erupted Volume				
Exponential[a] (km^3)	26.8×10^{-4}	2.8×10^{-1}	2.1×10^{-1}	4.9×10^{-1}
Break in slope I–II (BS_1, km)	–	10.4	4.2	24.5
Break in slope II–III (BS_2, km)	–	168.2	92.3	121.4
bt_1[b] (km)	0.7	3.3	0.8	6.2
bt_2[b] (km)	–	11.9	9.8	10.2
bt_3[b] (km)	–	43.9	24.8	37.6
Power-law[c] (km^3)	$55.1\pm0.2\times10^{-4}$	2.4×10^{-1}	1.4×10^{-1}	9.6×10^{-1}
Proximal limit (B, km)	1	1	1	1
Distal limit (C, km)	100–500	352	303	447
PL-coefficient (T_{PL})	271	1,126	212	15,451
PL-Exponent (m)	3.0	1.8	1.5	2.3
Ht[d] (km)	13	10	17–19	–
MER (kg/s)				
Peak[e]	9.2×10^6	3.2×10^6	4.2×10^7	–
Average[f]	1.2×10^5	–	–	–
Erupted Mass[g] (kg)				
Exponential derived	2.7×10^9	2.8×10^{11}	2.7×10^{11}	4.9×10^{11}
Power-law derived	$54.9\pm0.2\times10^8$	2.4×10^{11}	1.8×10^{11}	9.6×10^{11}
Duration[h]				
Exponential derived	5 min	24 h	2 h	–
Power-law derived	10 min	20 h	1 h	–
Volcanic Explosivity Index (VEI)	2	4	4	4
Magnitude[i]				
Exponential derived	2.4	4.4	4.4	4.7
Power-law derived	2.7 ± 0.4	4.4	4.3	5.0

[a]Calculated through integration of three segments for A-M, β and the total deposit; on one segment for α:

$$V = \frac{2T_{0,1}}{{k_1}^2} + 2T_{0,1}\left[\frac{k_2BS_1+1}{k_2^2} - \frac{k_1BS_1+1}{k_1^2}\right]\exp^{(-k_1BS_1)} + 2T_{0,2}\left[\frac{k_3BS_2+1}{k_3^2} - \frac{k_2BS_2+1}{k_2^2}\right]\exp^{(-k_2BS_2)} + \\ + \ldots + 2T_{0,(n-1)}\left[\frac{k_nBS_{(n-1)}+1}{k_n^2} - \frac{k_{(n-1)}BS_{(n-1)}+1}{k_{(n-1)}^2}\right]\exp^{(-k_{(n-1)}BS_{(n-1)})}$$

where $T_{0,n}$, $-k_n$ and BS_n are the intercept, slope and breack-in-slope of the line segment n (Bonadonna and Houghton 2005).

[b]$bt_n = \ln 2/k_n$; Half thickness distance of the line segment n (Pyle 1989).

[c]$V = \frac{2T_{PL}}{2-m}\left[C^{(2-m)} - B^{(2-m)}\right]$

where T_{PL} and m are the coefficient and exponent of the power-law, C and B are the proximal and distal limit of integration (Bonadonna and Houghton, 2005).

[d]Based on the calculation of Carey and Sparks (1986) applied to the 3.2 cm isopleths contour of the 3/5 average and 50th percentile strategies for Layer β. Ht of layers α and A-M are derived from remote sensing observations.

[e]Wilson and Walker (1987); the value for Layer β is referred to the column height calculated with the 3/5 average isopleths (i.e., 19 km) according to Carey and Sparks (1986); the values for layers α and A-M are referred to the column heights determined by remote sensing analyses (i.e., 13 and 10 km respectively) and reported by the Smithsonian Institute (Folch et al. 2008; Lara 2009).

[f]The average MER is calculated for Layer a from the observed eruption duration of the eruptive phase described by the SERNAGEOMIN report (i.e., 6 h).

[g]Calculated from the erupted volume considering a density of 1,250 kg/m^3 for Layer β (average of eleven measurements made in situ with a standart deviation of 50 kg/m^3) and a density of 997 kg/m^3 for layers α, A-M and the total deposit (Watt et al. 2009).

[h]Duration = Mass/MER.

[i]Magnitude = Log(Mass) − 7; (Pyle 2000).

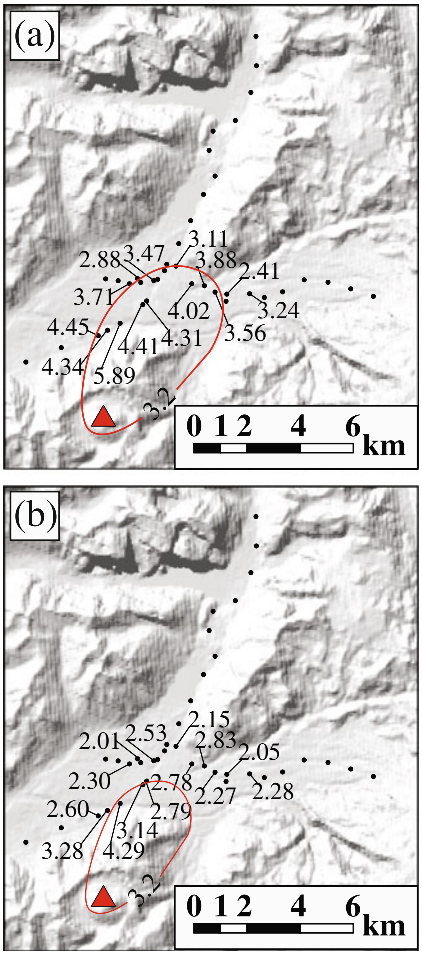

Fig. 7 Isopleth maps (cm) of Layer β compiled for **a** the average of the geometric mean of the three orthogonal axes of the 5 largest lithic clasts (3/5 average technique); **b** the geometric mean of the three orthogonal axes of the 50th percentile of the 20 largest lithic clasts. The 3.2 cm isoline is shown

determination of the volume more complex. By considering that the most distal isopach contour extends to 0.1 mm, the distal integration limit can be considered fixed.

The calculated cumulative volume of the whole deposit ranges between 4.9–9.6$\times 10^{-1}$ km^3 (obtained by integration of three exponential segments and power-law fit). The bulk volume for the whole deposit and for layers A-M (combined with the May 3rd lobe) and Layer β (combined with the May 6th lobe) are therefore both larger than the volumes estimated by Watt et al. (2009). In fact, Watt et al. (2009) derived a whole-deposit volume between 1.5$\times 10^{-1}$ km^3 and 1.7$\times 10^{-1}$ km^3, and a volume of 0.5$\times 10^{-1}$ km^3 and 0.3$\times 10^{-1}$ km^3 for the May 3rd and May 6th lobes respectively (by integration of a single exponential segment). Such a difference can be explained by the fact that the volumes estimated by Watt et al. (2009) do not account for the contribution of several eruptive events that only deposited in proximal/medial areas (<25 km from the vent); in addition, a smaller part of this volume difference reflects the slightly larger areas of our redrawn distal isopachs, when compared to those estimated by Watt et al. (2009). In fact, Chaitén activity has been characterized by a succession of weak to moderate explosions associated with tephra fall mainly in proximal/medial areas. As a result, only a relatively small fraction of the erupted material, produced by the largest explosive events and characterized by a fine grain size, was sedimented in the distal areas of Argentina (and was sampled by Watt et al. 2009).

Preliminary volume estimations for the 1st–6th May phase of the eruption based on remote sensing analysis and computer modeling resulted in larger values (i.e., 4 km^3, Lara 2009; 6 km^3 DRE, Folch et al. 2008). As pointed out both by Lara (2009) and Folch et al. (2008), these models overestimated the erupted volume because calculations used a constant plume height and MER for 6 days. In fact, when the brief duration of the Plinian phase is considered, remote sensing and modeling analysis also imply an eruptive volume of ~1 km^3 (Carn et al. 2009). Nonetheless, our stratigraphic analysis may underestimate the volume (i.e., 0.5–1.0 km^3) due to erosional processes occurring soon after deposition.

No significant erosion has occurred in between June 2008 and January 2009. In fact, the values of thickness observed in the area of Futaleufù at the time of our fieldwork were similar to the values observed in mid-June 2008 by Watt et al. (2009). Potential erosion might have occurred in between the start of the eruption and June 2008. However, first thicknesses estimates in the distal area of Futaleufù were only ~25% larger than those of Watt et al. (2009) (Amigo, personal commun.). Nonetheless, the overall modeled erupted volume based on an increased thickness in distal areas remains unvaried (1.0 km^3 both from exponential and power-law fits). We consider that proximal deposition in the forest during the first phase of the eruption was less affected by erosion due the coarser grainsize of the products, the rapid sedimentation and accumulation of multiple layers, reduced wind reworking and preservation by vegetation. In fact, with the exception of the top layers, the layers sampled in the forest did not show significant evidence of reworking. If 25% erosion is also considered in proximal areas, the resulting volume is 1.3 km^3

Eruption style

The May 2008 Chaitén eruption shows similar characteristics to the activity inferred for other volcanoes characterized by the extrusion of an obsidian rhyolitic dome, such as the silicic lava domes of Inyo Volcanic Chain (California, USA; Bursik 1993; Miller 1985). These vents erupted about 600 years ago, inferred on the basis of isopach maps of

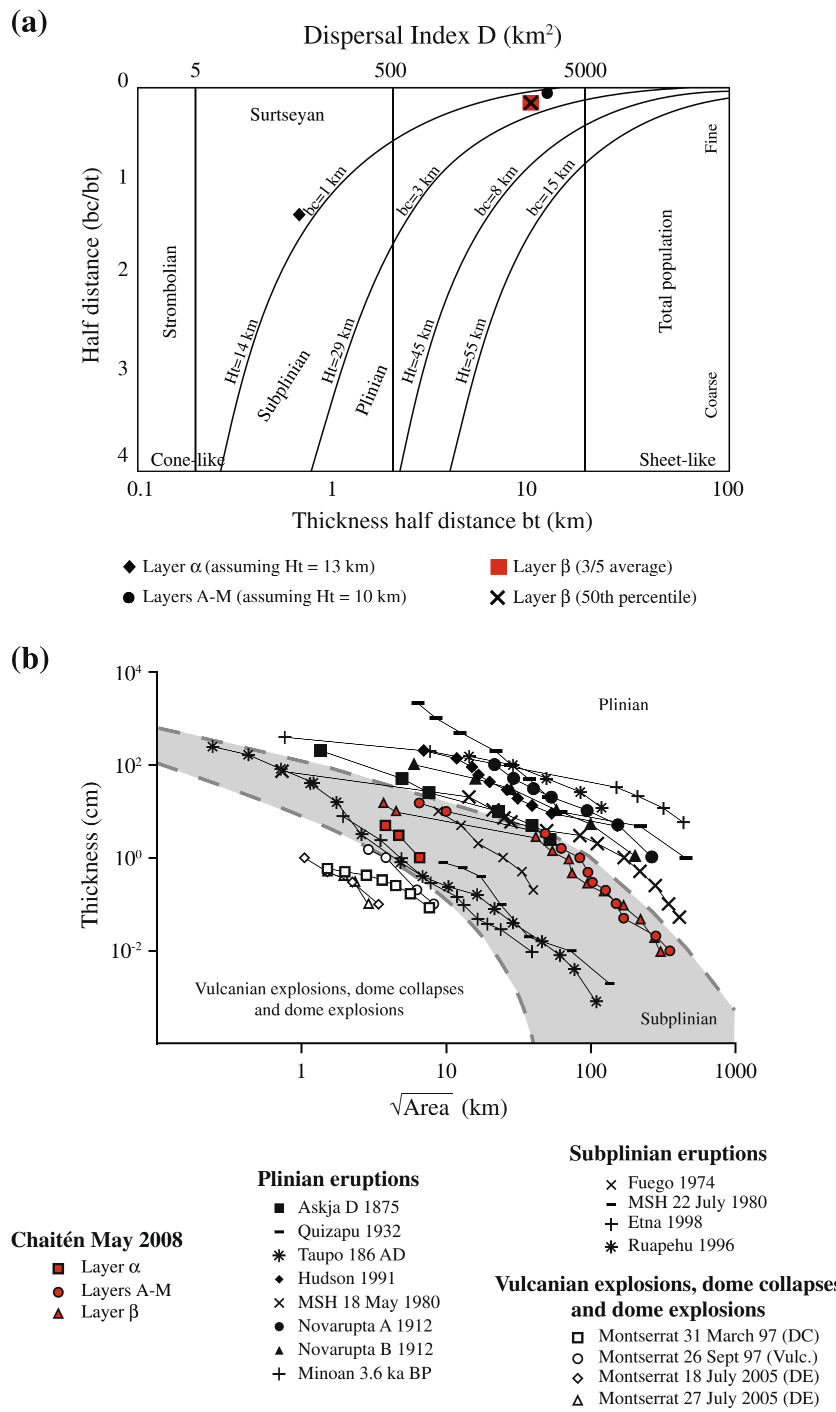

Fig. 8 **a** Classification plot for layers A-M, α, β according to Pyle (1989) using the bt_2 value (Table 2) related to the medial segment for Layers A-M, Layer β and the total deposit. **b** Comparison of the thinning trend of the layers α and β of the northern sector with other known eruption of different styles: Plinian eruptions: Askja 1975 (Sparks et al. 1981); Quizapu 1932, (Hildreth and Drake 1992); Taupo 186 AD, (Walker 1980); Hudson 1991, (Scasso et al. 1994); Mount St. Helens 18 May 1980, (Sarna-Wojcicki et al. 1981); Novarupta A and B 1912, (Fierstein and Hildreth 1992); Minoan 3.6 ka BP, (Pyle 1990), Subplinian eruptions: Fuego 1974, (Rose et al. 2008); Mount St. Helens 22 July 1980, (Sarna-Wojcicki et al. 1981); Etna 1998 (Bonadonna and Costa 2011); Ruapehu 1996 (Bonadonna et al. 2005), dome collapses (Montserrat 21 September 1997; Bonadonna et al. 2002), Vulcanian explosions (Montserrat 26 September 1997; Bonadonna et al. 2002), dome explosions (Montserrat 18 and 27 July 2005; this work)

tephra fall and PDC deposits to have produced weak subplinian explosions characterized by a maximum VEI 4 (tephra volume comprised between 0.5×10^{-1} and 1.0×10^{-1} km^3), but showing a wide dispersal of the products over a vast region (Miller 1985). In contrast, erupted volume of the May 2008 Chaitén eruption is significantly lower than that associated with Plinian rhyolitic eruptions. The 1991 eruption of Hudson volcano (Chile), for example, produced up to 7.6 km^3 of tephra (Scasso et al. 1994), the 1912 eruption of Novarupta (Alaska) generated about 17 km^3 of tephra (Houghton et al. 2004), while the prehistoric Taupo Plinian and Hatepe Plinian eruptions (both part of the Taupo eruption of 186AD) are associated with total volumes of 24 and 6 km^3 (Walker 1980, 1981).

Plume heights of the 2008 Chaitén eruption are also more similar to those of lava-dome eruptions than to those of large rhyolitic eruptions, such as Novarupta 1912 (Ht= 23–26 km; Hildreth and Drake 1992), Taupo 186 AD (Ht=

51 km; Walker 1980), Hatepe 186 AD (Ht=33 km; Walker 1981) and Waimihia 3500YBP (Ht=42 km; Walker 1981). As an example, the current eruption of Soufriere Hills volcano (Montserrat) has produced plumes with a maximum height of about 15 km for dome collapse, vulcanian explosions and the subplinian eruption of September 17th 1996 (Bonadonna et al. 2002; Robertson et al. 1998).

One interesting feature of the May 2008 Chaitén eruption is related to the composition of the products, which seems to have remained the same during all phases of activity, in contrast to the Novarupta 1912 eruption during which the products varied from rhyolitic to andesitic composition during the same eruption (Houghton et al. 2004). The high silica content, in fact, is the same for all the Chaitén layers analyzed, and is the same composition as the obsidian of the old dome (Table 1). However, the Novarupta eruption produced a much larger volume of tephra.

The case of Chaitén volcano seems to be also similar to Mount St. Helens volcano's 1980 activity, which started with a Plinian phase that produced a 19 km high plume (Holasek and Self 1995), erupting a volume of tephra equal to 1.1–1.3 km^3 (Bonadonna and Houghton 2005), followed by extrusion of a lava dome. However, the Mount St. Helens eruption was triggered by a sector collapse and was followed by a decrease in activity characterized by the extrusion of a dacitic dome over several years (Baxter et al. 1981).

Hazard implications

The prevailing winds in southern Chile are towards the E, as shown by the distribution of distal ash erupted during the May 2008 Chaitén eruption (Watt et al. 2009) as well as older tephra deposits (Naranjo and Stern, 2004). As a result Chaitén town was not significantly affected by tephra fall (Fig. 5). In fact, as of January 2009, <10 cm of tephra had accumulated in Chaitén town since the beginning of the eruption. In areas >5 km from the vent, continuous ash deposition generated by frequent but small-magnitude events mainly associated with dome growth are more likely to cause damage to vegetation and to every-day activity than building collapse (e.g., Bonadonna et al. 2002). This is even more true in the case where ash is systematically and frequently removed, which is recommended for buildings in the area proximal to the volcano. Nonetheless, if the deposition of Layer β had been directed towards Chaitén town, about 10 cm of tephra would have fallen there in just a few hours, causing collapse of the weakest buildings and major disruption of human activities. Finally, the continuous ash production significantly damaged the forest vegetation around Chaitén dome (NE of Parque Pumalin). The accumulation of a tephra deposit in distal areas also caused major disruption to agriculture and other human activities as far as the Atlantic coast of Argentina (~600 km from the dome). As an example, as verified by direct observations the tephra deposits in Futaleufù (75 km from the vent) and accounts of resident people, a few millimeters of ash were enough to cause the death of cattle and damage to crops. The volume erupted was also enough to cause the cancellation of hundreds of domestic flights in Chile and Argentina and to affect heavily the aquaculture industry nearby the Gulf of Corcovado (Watt et al. 2009; Carn et al. 2009).

We also identified approximately 1 m thick deposits of discontinuously laminated and reworked tephra along the thalweg of the Rio Michimahuida, more than 20 km from the volcano. These deposits are the product of rapid channel aggradation and overbank deposition from of sediment-rich flood waters. This valley is topographically isolated from Chaitén volcano and no PDCs reached the valley at any point during the eruption. Instead, the source of these flows is the rapid remobilization of the tephra fall deposits in this valley. Evidence of deposit erosion was abundant, even in areas where total tephra thickness was less than 10 cm. This evidence includes the development of meter-scale dendritic channels in the deposit, and concentration of large particles at the top of the deposit. Thus, lahar hazards at medial distances from the volcano were increased because of rapid deposit erosion, possibly due to decreased infiltration as function of the thickness and fine grainsize of the deposit (e.g., Collins and Dunne, 1986; Manville and Wilson, 2004; Volentik et al. 2009; Yamakoshi et al. 2005).

The Chaitén ash contains abundant ash in the respirable fraction (8.8–17.7 vol.% <4 μm diameter) and a significant amount of cristobalite (2–19 vol.%) both typically associated with extrusion of a rhyolitic dome (Reich et al. 2009; Horwell et al. 2010). Cristobalite typically forms in a lava-dome setting by devitrification of volcanic glass and, being the most toxic silica polymorph, long term exposure has the potential to cause serious illness, such as lung cancer and silicosis (i.e., Baxter et al. 1999; Horwell and Baxter 2006).

The current activity of Chaitén volcano is not delivering a significant amount of ash to populated areas. Ash remobilization, or/and potential increase in volcanic activity could, however, pose a health risk to the exposed populations.

Conclusions

The May 2008 rhyolitic eruption of Chaitén volcano was characterized by a rapid and energetic onset, followed by a weak waning phase, with associated dome-growth activity, and generation of PDCs and floods. The activity included two main subplinian events (which produced Layers α and β) both followed by a few days of continuous ash emission with very homogeneous composition (74–75% SiO_2). In fact, the eruption began with the subplinian explosion (VEI 2 – Magnitude 2.4) on May 1st–2nd, that deposited Layer α towards the NE. In the following days (May 3rd to May 5th), the eruption was characterized by a continuous emission of ash which produced a larger cumulative deposit (cumulative VEI 4 – Magnitude 4.5) characterized by several fine to coarse ash layers towards the E and SE. The distribution of these layers followed an anticlockwise shift in wind direction, from SE, on May 3rd (layers A-J), to E, on May 5th (layers K-M). The paroxysmal phase occurred on May 6th (VEI 4 – Magnitude 4.5) producing a subplinian plume up to 19 km, associated with a peak MER of about 4×10^7 kg/s, which lasted about 2–3 h, and deposited Layer β towards NE. The cumulative volume erupted during the main explosive phase is estimated to have been at least of ~0.5 km^3 bulk tephra volume. The post May 6th activity has been characterized by small explosions which produced the deposition of the ash to lapilli layers located N of the crater (layers χ–ν). The total bulk tephra volume erupted between 1st May 2008–January 2009 is about 0.5–1.0 km^3.

Preliminary analysis of sedimentary deposits in Chaiten town and other data suggest that damage to the town was caused primarily by rapid channel aggradation and diversion of a prolonged sediment-laden water flood into the town rather than by a single, large, highly concentrated lahar (Pierson, written commun., 2010). Therefore, the main current hazard for the populated areas of Chaitén town is the generation of sediment-rich floods from the remobilization of deposits from PDCs and fall deposits around the Chaitén dome. However, a shift of the wind direction towards SE and an increase in the frequency of explosive and dome collapse events could also result in a major disruption of the daily-life activities in Chaitén town related to the accumulation of tephra deposit in medial areas. Accumulation of tephra deposits in distal areas has already caused significant disruption to several socio-economic sectors, e.g. agriculture, tourism, aviation, human and animal health.

Acknowledgements F. Alfano was supported by an Augustin Lombard grant from the Société Physique et d'Histoire Naturelle (SPHN) society of Geneva and by the "Master and Back program" (Sardegna, Italy); C. Bonadonna was supported by Fonds Marc Birkigt (Geneva, Switzerland); A.C.M. Volentik, C.B. Connor and L.J. Connor were supported by a National Science Foundation (NSF) grant EAR 0838115, (USA); S.F.L. Watt and D.M. Pyle were supported by a Natural Environment Research Council UK (NERC) urgency grant (NE/G001715/1). H. Moreno is thanked for providing fruitful discussion and SERNAGEOMIN information on the first phase of the eruption. We thank Luis Lara and Larry Mastin for reviews that improved the manuscript.

References

Baxter PJ, Ing R, Falk H, French J, Stein GF, Bernstein RS, Merchant JA, Allard J (1981) Mount-St-Helens eruptions, May 18 to June 12, 1980—an overview of the acute health impact. Jama-J Am Méd Assoc 246(22):2585–2589

Baxter PJ, Bonadonna C, Dupree R, Hards VL, Kohn SC, Murphy MD, Nichols A, Nicholson RA, Norton G, Searl A, Sparks RSJ, Vickers BP (1999) Cristobalite in volcanic ash of the Soufrière Hills volcano, Montserrat, British West Indies. Sci 283 (5405):1142–1145

Bonadonna C, Costa A (2011) Modeling of tephra sedimentation from volcanic plumes. In: Fagents S, Gregg T, Lopes R (eds) Modeling volcanic processes: The physics and mathematics of volcanism. Cambridge University Press

Bonadonna C, Houghton BF (2005) Total grainsize distribution and volume of tephra-fall deposits. Bull Volcanol 67:441–456

Bonadonna C, Mayberry GC, Calder ES, Sparks RSJ, Choux C, Jackson P, Lejeune AM, Loughlin SC, Norton GE, Rose WI, Ryan G, Young SR (2002) Tephra fallout in the eruption of Soufrière Hills volcano, Montserrat. In: Druitt TH, Kokelaar BP (eds) The eruption of Soufrière Hills volcano, Montserrat, from 1995 to 1999. Memoir Geological Society, London, pp 483–516

Bonadonna C, Phillips JC, Houghton BF (2005) Modeling tephra sedimentation from a Ruapehu weak plume eruption. J Geophys Res 110 (B8, B08209)

Bursik M (1993) Subplinian eruption mechanisms inferred from volatile and clast dispersal data. J Volcanol Geotherm Res 57(1–2):57–70

Carey SN, Sparks RSJ (1986) Quantitative models of the fallout and dispersal of tephra from volcanic eruption columns. Bull Volcanol 48:109–125

Carn SA, Pallister JS, Lara L, Ewert JW, Watt S, Prata AJ, Thomas RJ, Villarosa G (2009) The unexpected awakening of Chaitén volcano, Chile. EOS, Trans Am Geophys Union 90 (24). doi:10.1029/2009EO240001

Castro JM, Dingwell DB (2009) Rapid ascent of rhyolitic magma at Chaitén volcano, Chile. Nat 461(7265):780–783

Cembrano J, Lara L (2009) The link between volcanism and tectonics in the southern volcanic zone of the Chilean Andes: a review. Tectonophys 471(1–2):96–113

Collins BD, Dunne T (1986) Erosion of tephra from the 1980 eruption of Mount St. Helens, Geol Soc Am Bull 97:896–90

Fierstein J, Hildreth W (1992) The plinian eruptions of 1912 at Novarupta, Katmai national park, Alaska. Bull Volcanol 54:646–684

Folch A, Jorba O, Viramonte J (2008) Volcanic ash forecast—application to the may 2008 Chaitén eruption. Nat Hazards Earth Syst Sci 8(4):927–940

Hildreth W, Drake RE (1992) Volcano Quizapu, Chilean Andes. Bull of Volcanol 54:93–125

Holasek RE, Self S (1995) Goes weather-satellite observations and measurements of the May 18, 1980, Mount-St-Helens eruption. J Geophys Res-Solid Earth 100(B5):8469–8487

Horwell CJ, Baxter PJ (2006) The respiratory health hazards of volcanic ash: A review for volcanic risk mitigation. Bull Volcanol 69(1):1–24. doi:10.1007/s00445-006-0052-y

Horwell CJ, Le Blond JS, Michnowicz SAK, Cressey G (2010) Cristobalite in a rhyolitic lava dome: evolution of ash hazard. Bull Volcanol 72(2):249–253. doi:10.1007/s00445-009-0327-1

Houghton BF, Wilson CJN, Fierstein J, Hildreth W (2004) Complex proximal deposition during the plinian eruptions of 1912 at Novarupta, Alaska. Bull Volcanol 66(2):95–133

Lange D, Cembrano J, Rietbrock A, Haberland C, Dahm T, Bataille K (2008) First seismic record for intra-arc strike-slip tectonics along the Liquine-Ofqui fault zone at the obliquely convergent plate margin of the southern Andes. Tectonophys 455(1–4):14–24. doi:10.1016/j.tecto.2008.04.014

Lara LE (2009) The 2008 eruption of the Chaiten volcano, Chile: a preliminary report. Andean Geol 36(1):125–129

Manville V, Wilson CNJ (2004) The 26.5 ka Oruanui eruption, New Zealand: a review of the roles of volcanism and climate in the post-eruptive sedimentary response. New Zeal J Geol Geophys 47:525–547

Martin RS, Watt SFL, Pyle DM, Mather TA, Matthews NE, Georg RB, Day JA, Fairhead T, Witt MLI, Quayle BM (2009) Environmental effects of ashfall in Argentina from the 2008 Chaitén volcanic eruption. J Volcanol Geotherm Res 184(3–4):462–472

Miller CD (1985) Holocene eruptions at the Inyo volcanic chain, California—implications for possible eruptions in Long Valley caldera. Geol 13(1):14–17

Naranjo JA, Stern CR (2004) Holocene tephrochronology of the southernmost part (42 degrees 30′–45 degrees s) of the Andean southern volcanic zone. Rev Geol Chile 31(2):225–240

Pyle DM (1989) The thickness, volume and grainsize of tephra fall deposits. Bull Volcanol 51(1):1–15

Pyle DM (1990) New estimates for the volume of the Minoan eruption. In: Hardy DA (ed) Thera and the aegean world, vol III. The Thera Foundation, London, pp 113–121

Pyle DM (1995) Assessment of the minimum volume of tephra fall deposits. J Volcanol Geotherm Res 69(3–4):379–382

Pyle DM (2000) Sizes of volcanic eruptions. In: Sigurdsson H, Houghton B, Rymer H, Stix J, McNutt S (eds) Encyclopedia of volcanoes. Academic, San Diego, pp 263–270

Reich M, Zuniga A, Amigo A, Vargas G, Morata D, Palacios C, Parada MA, Garreaud RD (2009) Cristobalite nanofibers in volcanic ash from the ongoing explosive eruption at Chaitén volcano, Chilean Patagonia. Geochim Cosmochim Acta 73(13):A1083–A1083

Robertson R, Cole P, Sparks RSJ, Harford C, Lejeune AM, McGuire WJ, Miller AD, Murphy MD, Norton G, Stevens NF, Young SR (1998) The explosive eruption of Soufrière Hills volcano, Montserrat, West Indies, 17 september, 1996. Geophys Res Lett 25(18):3429–3432

Rose WI, Self S, Murrow PJ, Bonadonna C, Durant AJ, Ernst GGJ (2008) Nature and significance of small volume fall deposits at composite volcanoes: Insights from the October 14, 1974 Fuego eruption, Guatemala. Bull Volcanol 70(9):1043–1067. doi:10.1007/s00445-007-0187-5

Sarna-Wojcicki AM, Shipley S, Waitt JR, Dzurisin D, Wood SH (1981) Areal distribution thickness, mass, volume, and grain-size of airfall ash from the six major eruptions of 1980. In: Lipman WP, Mullineaux DR (eds) Eruptions of Mount St. Helens, Washington, vol 1250. U.S. Geological Survey Professional Paper Washington, D.C., pp 577–600

Scasso R, Corbella H, Tiberi P (1994) Sedimentological analysis of the tephra from 12–15 August 1991 eruption of Hudson volcano. Bull Volcanol 56:121–132

Sparks RSJ, Wilson L, Sigurdsson H (1981) The pyroclastic deposits of the 1875 eruption of Askja, Iceland. Philos Trans R Soc Lond 229:241–273

Stern CR, Garcia C, Navarro X, Munoz J (2009) Sources and distribution of different types of obsidian from archaeological sites in central-south Chile (38–44 degrees s). Magallania 37 (1):179–192

Volentik ACM, Connor CB, Connor LJ, Bonadonna C (2009) Aspects of volcanic hazard assessment for the Bataan nuclear power plant, Luzon peninsula, Philippines. In: Connor CB, Chapman N, Connor LJ (eds) Volcanic and tectonic hazard assessment for nuclear facilities. Cambridge University Press, Cambridge, pp 229–256

Walker GPL (1980) The Taupo pumice: product of the most powerful known (ultraplinian) eruption. J Volcanol Geotherm Res 8:69–94

Walker GPL (1981) The Waimihia and Hatepe plinian deposits from the rhyolitic taupo volcanic centre. New Zealand J Geol Geophys 24:305–324

Watt SFL, Pyle DM, Mather TA, Martin RS, Matthews NE (2009) Fallout and distribution of volcanic ash over Argentina following the May 2008 explosive eruption of Chaitén, Chile. J Geophys Res-Solid Earth 114:11. doi:B0420710.1029/2008jb006219

Wilson L, Walker GPL (1987) Explosive volcanic-eruptions.6. Ejecta dispersal in plinian eruptions—the control of eruption conditions and atmospheric properties. Geophys J R Astron Soc 89(2):657–679

Yamakoshi T, Doi Y, Osanai N (2005) Post-eruption hydrology and sediment discharge at the Miyakejima volcano, Japan. In: Thouret JC, Chester DK (eds) Volcanic landforms, processes and hazards, vol 140. Zeitschrift fur geomorphologie supplement series. Gebruder Borntraeger, Stuttgart, pp 55–72